Mechanisms of Alveolar Epithelial Translocation of a Defined Population of Nanoparticles

Nazanin R. Yacobi[1,6], Noah Malmstadt[1], Farnoosh Fazlollahi[1,6], Lucas DeMaio[2,6], Ronald Marchelletta[3], Sarah F. Hamm-Alvarez[3], Zea Borok[2,4,6], Kwang-Jin Kim[2,3,6], and Edward D. Crandall[1,2,5,6]

[1]Mork Family Department of Chemical Engineering and Materials Science, [2]Department of Medicine, [3]Department of Pharmacology and Pharmaceutical Sciences, [4]Department of Biochemistry and Molecular Biology, [5]Department of Pathology, and [6]Will Rogers Institute Pulmonary Research Center, University of Southern California, Los Angeles, California

To explore mechanisms of nanoparticle interactions with and trafficking across lung alveolar epithelium, we utilized primary rat alveolar epithelial cell monolayers (RAECMs) and an artificial lipid bilayer on filter model (ALBF). Trafficking rates of fluorescently labeled polystyrene nanoparticles (PNPs; 20 and 100 nm, carboxylate (negatively charged) or amidine (positively charged)-modified) in the apical-to-basolateral direction under various experimental conditions were measured. Using confocal laser scanning microscopy, we investigated PNP colocalization with early endosome antigen–1, caveolin-1, clathrin heavy chain, cholera toxin B, and wheat germ agglutinin. Leakage of 5-carboxyfluorescein diacetate from RAECMs, and trafficking of ^{22}Na and ^{14}C-mannitol across ALBF, were measured in the presence and absence of PNPs. Results showed that trafficking of positively charged PNPs was 20–40 times that of negatively charged PNPs across both RAECMs and ALBF, whereas translocation of PNPs across RAECMs was 2–3 times faster than that across ALBF. Trafficking rates of PNPs across RAECMs did not change in the presence of EGTA (which decreased transepithelial electrical resistance to zero) or inhibitors of endocytosis. Confocal laser scanning microscopy revealed no intracellular colocalization of PNPs with early endosome antigen–1, caveolin-1, clathrin heavy chain, cholera toxin B, or wheat germ agglutinin. Leakage of 5-carboxyfluorescein diacetate from alveolar epithelial cells, and sodium ion and mannitol flux across ALBF, were not different in the presence or absence of PNPs. These data indicate that PNPs translocate primarily transcellularly across RAECMs, but not via known major endocytic pathways, and suggest that such translocation may take place by diffusion of PNPs through the lipid bilayer of cell plasma membranes.

Keywords: epithelial transport; lipid bilayers; cell monolayers; particle trafficking; pneumocytes

Advances in nanotechnology have led to expanded applications in industry and biomedicine, while raising increased concerns about health effects of nano-sized materials (diameter $\leqslant$100 nm). Inhaled ambient ultrafine particles (diameter $<$100 nm) have been associated with adverse cardiovascular and other health effects (1–3), and have been found downstream in internal organs (4). Since the alveolar epithelial barrier provides more than 95% of the total surface area of the airspaces in the lung (5, 6), and the effective thickness of the distal air–blood barrier is very thin ($\sim$400 nm) (7), alveolar epithelium likely plays an important role in absorption of inhaled nanomaterials into the systemic circulation (4). Investigation of mechanisms underlying nanoparticle interactions with and translocation across alveolar epithelium will provide important information on lung–nanoparticle interactions, and may lead to improved nanoparticle design for biomedical applications targeting the lung (e.g., pulmonary drug/gene delivery).

Distal airspaces of the lung are lined with a continuous epithelium comprised of two types of alveolar epithelial cells (AECs), type I (ATI) and type II (ATII) pneumocytes. Extremely thin cytoplasmic extensions of ATI cells are thought to facilitate efficient gas exchange (8). About 90% of the internal surface area of the normal human lung is covered by ATI cells. Specific mechanistic information pertaining to alveolar epithelial barrier properties and trafficking rates of macromolecules and nanoparticles is difficult to obtain from data generated with whole-lung preparations *in vivo* or isolated perfused lungs, primarily due to the complex anatomy of the lung. *In vitro* models for alveolar epithelium have been widely used to study important biological and functional characteristics (9, 10). Primary cultured rat ATII cells are known to undergo morphologic (5) and phenotypic (11) transition into ATI cell–like monolayers that can serve as a suitable *in vitro* model of the alveolar epithelial barrier for mechanistic investigations of transport and cell biology. Rat alveolar epithelial cell monolayers (RAECMs) exhibit relatively high transepithelial resistance (transmonolayer electrical resistance (Rt) $>$2,000 $\Omega \cdot cm^2$), with well formed tight junctions, consistent with the expected properties of alveolar epithelium *in vivo*.

Artificial lipid bilayers have been used as model systems for the evaluation of membrane transport processes. When a porous filter surface is coated with lipid solution in hydrocarbon solvent and contacted with electrolyte solution on both sides, lipid bilayers form (12). Such artificial lipid bilayers on filters (ALBFs) have been used in numerous studies to estimate transcellular permeation of small molecules and peptides (13, 14). Using an artificial lipid bilayer construct containing lipid components in proportions similar to the lipid components of rat AEC plasma membranes (15, 16) may provide useful information related to interactions of nanoparticles with AEC plasma membranes.

We have recently shown that transport of polystyrene nanoparticles (PNPs) across RAECMs is strongly dependent on PNP surface properties and size, where amidine-modified (positively charged) PNPs are translocated across RAECMs 20- to 40-times faster than similarly sized carboxylate-modified (negatively charged) PNPs (17). The aim of the present study was to investigate mechanisms of transalveolar epithelial trafficking of PNPs with different physicochemical characteristics with RAECMs as an *in vitro* model of alveolar epithelium. We studied effects of EGTA, inhibitors of endocytosis, and co-incubation with cationic polypeptides on PNP trafficking rates across RAECMs. We also investigated characteristics of PNP translocation across ALBFs with lipid compositions resembling those of rat AEC plasma membranes. Results indicate that PNPs

(*Received in original form April 23, 2009 and in final form June 12, 2009*)

This work was supported in part by the Hastings Foundation, Whittier Foundation, and research grants EY 11386, EY 17923, ES 17034, ES 18782, HL 38578, HL 38621, HL 38658, HL 62569, HL 64,365, and HL89445 from the National Institutes of Health, and 0730280N from the American Heart Association.

Correspondence and requests for reprints should be addressed to Edward D. Crandall, Ph.D., M.D., Department of Medicine, University of Southern California, IRD 620, 2020 Zonal Avenue, Los Angeles, CA 90033. E-mail: ecrandal@usc.edu

Am J Respir Cell Mol Biol Vol 42. pp 604–614, 2010
Originally Published in Press as DOI: 10.1165/rcmb.2009-0138OC on July 2, 2009
Internet address: www.atsjournals.org

translocate across RAECMs primarily via nonendocytic transcellular pathways, and that PNP translocation across ALBFs exhibits properties similar to those across RAECMs, suggesting that PNP trafficking across alveolar epithelium may involve direct interaction with lipid bilayers of AEC plasma membranes.

MATERIALS AND METHODS

RAECM

The detailed procedure for routine preparation of RAECMs has been described previously (18, 19). This method involving the usage of rats has been approved by the Institutional Animal Care and Use Committee of the University of Southern California. Briefly, ATII pneumocytes were isolated from adult male, specific pathogen-free, Sprague-Dawley rats (125–150 g) with elastase digestion and enriched by IgG panning (18, 19). Enriched ATII cells were plated onto tissue culture–treated polycarbonate filters (Transwell, 12 mm diameter, 0.4 μm diameter pores; Corning-Costar, Cambridge, MA) at 1.2×10^6 cells/cm^2. In most experiments, cells were cultured in MDS (comprised of serum-free defined medium (MDSF) supplemented with 10% newborn bovine serum (Omega, Tarzana, CA)). MDSF consists of a 1:1 mixture of Dulbecco's modified Eagle's medium and Ham's F-12 medium (Sigma, St. Louis, MO) supplemented with 1 mM nonessential amino acids (Sigma), 100 U/ml primocin (InvivoGen, San Diego, CA), 10 mM N-(2-hydroxyethyl)piperazine-N′-(2-ethanesulfonic acid) hemisodium salt (Sigma), 1.25 mg/ml BSA (BD Bioscience, San Jose, CA), and 2 mM L-glutamine (Sigma). Cells were maintained at 37°C in a humidified atmosphere of 5% CO_2 plus 95% air, and fed every other day starting on Day 3 in culture when confluent monolayers were formed. We utilized RAECMs at 4–7 days in culture, the Rt and potential difference (PD) of which were greater than 2.5 kΩ·cm^2 and greater than 10 mV, respectively, when screened with a Millicell-ERS device (Millipore, Bedford, MA).

ALBFs

Mimicking the lipid composition reported for plasma membranes of rat AEC (15, 16), a stock solution of a lipid mixture, comprised of 1.5% phosphatidylcholine, 0.6% phosphatidylethanolamine, 0.3% sphingomyelin, and 0.6% cholesterol (Avanti Polar Lipids, Alabaster, AL) in 1:1 (volume) mixture of squalene and decane (Sigma), was prepared. The upper surfaces of tissue culture–treated polycarbonate filters (Transwell, 12 mm diameter, 0.4 μm diameter pores) were covered by 0.1 ml of the stock lipid solution. Immediately (<10 s) after covering the upper surface with lipid solution, 0.4 ml and 1.5 ml MDS was added to the upper and lower compartments of the filters, respectively, to form ALBFs. ALBFs were maintained at 37°C in a humidified atmosphere of 5% CO_2 plus 95% air. The electrical resistance of ALBFs from Day 0 was greater than the maximum measurable (20 kΩ·cm^2) using the Millicell-ERS device.

Nanoparticles

Fluorescently labeled PNP (Invitrogen, Eugene, OR) that were either carboxylate-modified (i.e., negatively charged; diameters of 20 and 100 nm, with −304.3 and −320 μEq/g, respectively) or amidine-modified (i.e., positively charged; diameters of 20 and 120 nm, with 80.2 and 39.7 μEq/g, respectively) were used unless otherwise noted. Excitation/emission wavelengths of carboxylate- and amidine-modified PNPs are 580/605 and 490/515 nm, respectively.

PNP Translocation

PNP suspensions in working stocks were sonicated briefly (~2 min) prior to use until a clear solution was observed with the naked eye. Apical (upper) fluid was replaced with fresh media containing PNPs (apical [PNPs] = 176 μg/ml) and apical-to-basolateral flux (rate of flow) was estimated by monitoring PNP accumulation over time in basolateral (lower) fluid. At the end of each experiment, apical (upper) compartment fluid was sampled for measurement of PNP concentration (to verify minimal decrease from initial value). Concentrations of PNPs were estimated fluorometrically (SpectraMax M2; Molecular Devices, Sunnyvale, CA). Standard curves were generated using solutions with known concentrations of PNPs. Increases in basolateral (lower) fluid (PNPs) from 0 to 24 hours were used to calculate PNP flux, as described previously (17).

Effects of Reduced Rt

To determine the effects of "leakier" tight junctions (increased tight junctional conductance) on trafficking rates of PNPs across RAECMs, PNP flux was measured in the presence of 2 mM ethylene glycol-bis-(2-aminoethyl)-N,N,N′,N′-tetraacetic acid (EGTA; Sigma) in both apical and basolateral fluids. RAECMs were treated with EGTA for 30 minutes, after which monolayers were incubated with apical media containing different PNPs (20 and 100 nm carboxylate modified or 20 and 120 nm amidine modified; 176 μg/ml), while keeping EGTA (2 mM) present in both apical and basolateral fluids. Control monolayers were exposed to amidine-modified (20 and 120 nm) or carboxylate-modified (20 and 100 nm) PNPs (176 μg/ml) without EGTA. Flux of PNPs was measured subsequently, as described above. During EGTA exposure, bioelectric properties were determined over time.

Effects of Endocytosis Inhibitors

Effects of inhibiting caveolin-mediated endocytosis were evaluated with methyl-β-cyclodextrin (23). Monodansylcadaverine and chlorpromazine were used to disrupt clathrin-mediated endocytosis (20–22). Phagocytosis and macropinocytosis were inhibited by F-actin depolymerizing agents, latrunculin B and cyctochalasin D (21). Dynasore was used to disrupt dynamin-dependent endocytosis (including clathrin- and caveolin-mediated endocytosis) (24). Briefly, RAECMs were incubated with methyl-β-cyclodextrin (10–200 μM; Sigma), monodansylcadaverine (200 μM; Sigma), chlorpromazine (28 μM; Sigma), latrunculin B (20 μM; Sigma), cyctochalasin D (10 μM; Sigma), or dynasore (80 μM; Sigma) in both apical and basolateral fluids for 30 minutes. RAECMs were then exposed to apical amidine-modified (20 and 120 nm) or carboxylate-modified (20 and 100 nm) PNPs (176 μg/ml), and flux of PNPs were measured. Inhibitors were present in both apical and basolateral fluids throughout the duration of these experiments. Control monolayers were exposed to amidine-modified (20 and 120 nm) or carboxylate-modified (20 and 100 nm) PNPs (176 μg/ml) without inhibitors. As positive controls, flux of 50 μg/ml FITC–cholera toxin B (CTB; Sigma), which uses caveolae-mediated endocytosis (25) or 500 μg/ml Alexa 594-transferrin (Invitrogen), which uses clathrin-mediated endocytosis (25), was measured in the presence and absence of inhibitor(s).

Effects of Cationic Polypeptides

Polycationic substances, such as protamine (molecular weight, ~4,100) or poly-l-lysine (molecular weight, ~4,200) have been shown to compete for cell membrane binding with cationic molecules/peptides/particles and inhibit their adsorptive uptake in different cell types (26, 27). RAECMs were incubated with MDSF supplemented with protamine (1 mM; Sigma) or poly-l-lysine (1 mM; Sigma) in apical fluid for 30 minutes. RAECMs were then incubated with apical amidine-modified (20 and 120 nm) or carboxylate-modified (20 and 100 nm) PNPs (176 μg/ml), keeping protamine or poly-l-lysine present while flux of PNPs was measured. Control monolayers were exposed to amidine-modified (20 and 120 nm) or carboxylate-modified (20 and 100 nm) PNPs (176 μg/ml) without these polypeptides. As positive control, flux of 90 μg/ml Alexa 594–wheat germ agglutinin (WGA; Sigma), which uses adsorptive endocytosis (28), was measured in the presence and absence of protamine and poly-l-lysine.

Immunofluorescence and Confocal Fluorescence Microscopy

RAECMs were exposed to 176 μg/ml amidine-modified (120 nm) or carboxylate-modified (100 nm) PNPs with or without CTB (50 μg/ml; Alexa 594 or Alexa 488 labeled; Invitrogen) or WGA (50 μg/ml; Alexa 594 or Alexa 488 labeled; Sigma) for 1 or 2 hour(s) and processed for confocal laser scanning microscopy (CLSM). Exposed monolayers were washed with ice-cold PBS (pH 7.2) and fixed in 3.7% formaldehyde (J.T. Baker, Phillipsburg, NJ) for 15 minutes. Monolayers were then treated with 0.5% Triton X-100 (TX-100; Bio-Rad, Hercules, CA) for 15 minutes at room temperature, rinsed with PBS, and mounted on microscope slides (Curtin Matheson Scientific, Baltimore, MD) with

Vectashield mounting medium containing 4′,6-diamidino-2-phenylindole (DAPI) (Vector, Burlingame, CA).

In some experiments, monolayers were pretreated with EGTA (2 mM) for 30 minutes before exposure to amidine-modified (120 nm) or carboxylate-modified (100 nm) PNPs (176 μg/ml) for 24 hours. After rinsing with ice-cold PBS, monolayers were blocked with 5% BSA and 0.2% TX-100 in PBS at room temperature for 1 hour. Rabbit antibody against midregion human zonula occludens-1 (1:100; Zymed Laboratories, San Francisco, CA) in 1% BSA in PBS was added to fixed monolayers overnight at 4°C, followed by incubating monolayers with secondary antibody (goat anti-rabbit conjugated to Alexa 594 or Alexa 488; Invitrogen) in 1% BSA in PBS for 1 hour at room temperature. Monolayers were then rinsed with PBS and mounted on microscope slides with mounting medium containing DAPI.

For caveolin-1 or early endosome antigen–1 (EEA1) staining, RAECMs were exposed to 176 μg/ml amidine-modified (120 nm) or carboxylate-modified (100 nm) PNPs, 50 μg/ml CTB or 50 μg/ml WGA for 1 or 2 hours, fixed with 3.7% formaldehyde, permeabilized with 0.5% TX-100, and blocked with 5% BSA and 0.2% TX-100 in PBS. For clathrin heavy chain staining, RAECMs were fixed and permeabilized with ice-cold ethanol for 5 minutes at 20°C and blocked with 5% BSA and 0.2% TX-100 in PBS. Goat antibody against the N-terminus of human EEA1 (1:100; Santa Cruz Biotechnology, Santa Cruz, CA), or mouse antibodies against human caveolin-1 (1:100; BD Biosciences, San Jose, CA) or clathrin heavy chain (1:1; BD Biosciences), in 1% BSA in PBS was added to fixed monolayers overnight at 4°C. This was followed by incubating monolayers with the appropriate secondary antibody (e.g., goat anti-mouse or donkey anti-goat antibody labeled with either Alexa 594 or Alexa 488; Invitrogen) in 1% BSA in PBS for 1 hour at room temperature. Monolayers were then rinsed with PBS and mounted on microscope slides with mounting medium containing DAPI. Control monolayers (i.e., not exposed to PNPs; incubated with primary antibody or secondary antibody) were similarly processed.

Images were acquired with a Zeiss laser scanning microscope 510 Meta NLO CLSM imaging system (Zeiss, Jena, Germany) equipped with argon and red/green HeNe lasers mounted on a vibration-free table and attached to an incubation chamber.

5-Carboxyfluorescein Diacetate Leakage from RAECM

5-Carboxyfluorescein diacetate (5-CFDA) acetoxymethyl ester (AM) is a cell-permeant molecule that rapidly enters cells. Hydrolysis by intracellular esterases results in highly charged and fluorescent 5-CFDA that leaks out of cells slowly. RAECMs were loaded from the apical side with 5 mM 5-CFDA–AM (Invitrogen) for 1 hour. Excess 5-CFDA–AM in apical fluid was removed and RAECMs were exposed to 176 μg/ml nonfluorescent carboxylate-modified (i.e., diameters of 20 and 100 nm with −693.6 and −77.3 μEq/g, respectively; Invitrogen) or amidine-modified (i.e., diameters of 20 and 100 nm with 87.7 and 33.9 μEq/g, respectively; Invitrogen) PNPs. Control monolayers were exposed to 0.1% TX-100 (positive control) or fresh MDS (negative control). After 30 minutes and 2 hours, apical fluid was sampled, and the fluorescence intensity of 5-CFDA that leaked into apical fluid was estimated fluorometrically (SpectraMax M2) at excitation and emission wavelengths of 494 and 518 nm, respectively.

^{14}C-Mannitol and ^{22}Na Permeability across ALBFs

We measured the apparent permeability coefficient (P_{app}) across ALBFs of sodium, and a small hydrophilic solute (mannitol; 180 Da; ~0.82 nm) in the presence and absence of PNPs. P_{app} of sodium and mannitol were determined with ^{22}Na (Perkin Elmer, Boston, MA) and ^{14}C-mannitol (GE Healthcare, Buckinghamshire, UK), respectively. Upper-compartment fluid 24 hours after ALBF formation was replaced with fresh MDS containing PNPs (amidine- or carboxylate-modified; 20, 100, or 120 nm; apical [PNPs] ~176 μg/ml). ^{22}Na (apical [^{22}Na], ~2 μCi/ml) or ^{14}C-mannitol (apical [^{14}C-mannitol], ~0.67 μCi/ml) was added to upper-compartment fluid immediately after PNP (176 μg/ml) exposure. Control ALBFs were exposed to ^{22}Na or ^{14}C-mannitol in the absence of PNPs. Samples (100 μl) of lower-compartment fluid were collected 24 hours after ^{22}Na or ^{14}C-mannitol instillation. Samples (25 μl) were collected from upper-compartment fluid at 30 minutes and 24 hours for determination of upstream radioactivity. Radioactive samples were mixed with 10 ml Ecoscint (National Diagnostics, Atlanta, GA) and assayed with a β counter (Beckman Instruments, Fullerton, CA). P_{app} was estimated from the relationship $P_{app} = [A/(S*\Delta t)]/C_o$, where A is amount of ^{22}Na or ^{14}C-mannitol in lower compartment fluid, S is nominal surface area of ALBFs (1.13 cm^2), Δt is the length of time over which measurements are made and C_o is ^{22}Na or ^{14}C-mannitol concentration in upper compartment fluid.

Relative Hydrophobicity

Relative surface hydrophobicity of PNPs was evaluated with a protocol modified from that of Muller and colleagues (29). Briefly, adsorption of a hydrophobic dye, Rose Bengal (Sigma), to the surface of PNPs was estimated as follows. Increasing concentrations of PNPs (total volume of up to 75 μl) were mixed with 3 ml of Rose Bengal (150 μg) solution in PBS. Samples containing Rose Bengal with or without PNPs were then incubated for 5 hours with constant shaking (60 oscillations/min) at 37°C, followed by centrifugation for 50 minutes at 1,500 × *g* (Sorvall Legend RT Centrifuge; Thermo Fisher Scientific, Waltham, MA). Centrifuged samples yielded a two-phase system in which the pelleted PNPs with adsorbed Rose Bengal are in one phase, and the bulk medium (or supernatant) represents the other phase. We measured Rose Bengal in the supernatant at an absorption wavelength of 550 nm. Standard curves were constructed using known concentrations of Rose Bengal. The amount of Rose Bengal adsorbed to the surface of PNPs was then calculated by subtracting the total amount of Rose Bengal in the supernatant from the initial 150 μg. The partition coefficient of Rose Bengal was calculated as the ratio of the amount of Rose Bengal bound to the surfaces of PNPs to that found in corresponding supernatant. The plot of partition coefficient against total surface area

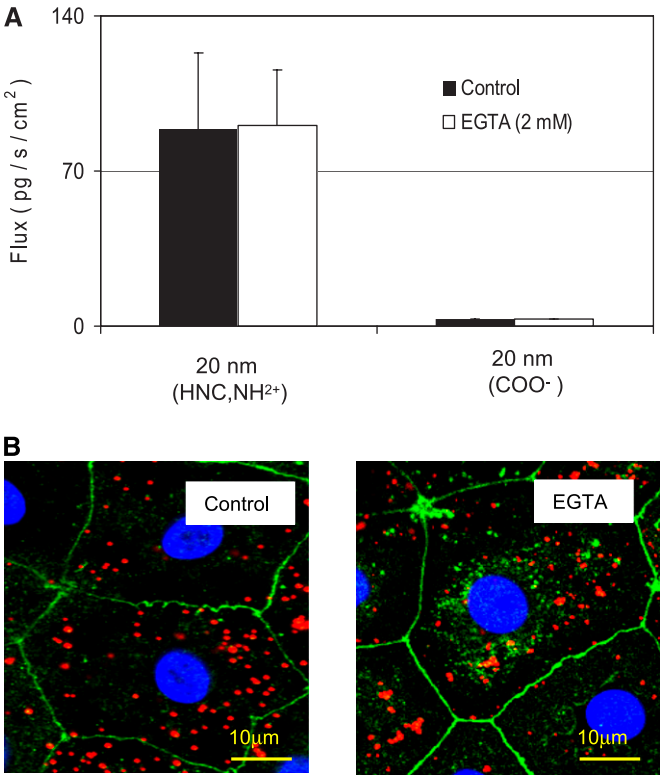

Figure 1. Effects of EGTA on polystyrene nanoparticles (PNPs) translocation across rat alveolar epithelial cell monolayer (RAECM). (*Panel A*) PNP (20 nm) (amidine-modified and carboxylate-modified) flux across EGTA-treated and nontreated (control) RAECMs exposed to176 μg/ml apical [PNPs] at time t = 0 (*n* = 6–9). (*Panel B*) Midsection confocal photomicrographs of control RAECMs and RAECMs treated with 2 mM EGTA exposed to 176 μg/ml apical [PNP] (100 nm; carboxylate-modified in *red*) for 24 hours. Cell–cell borders (zonula occludens-1 staining) and nuclei (4′,6-diamidino-2-phenylindole (DAPI) staining) are seen as *green* and *blue,* respectively.

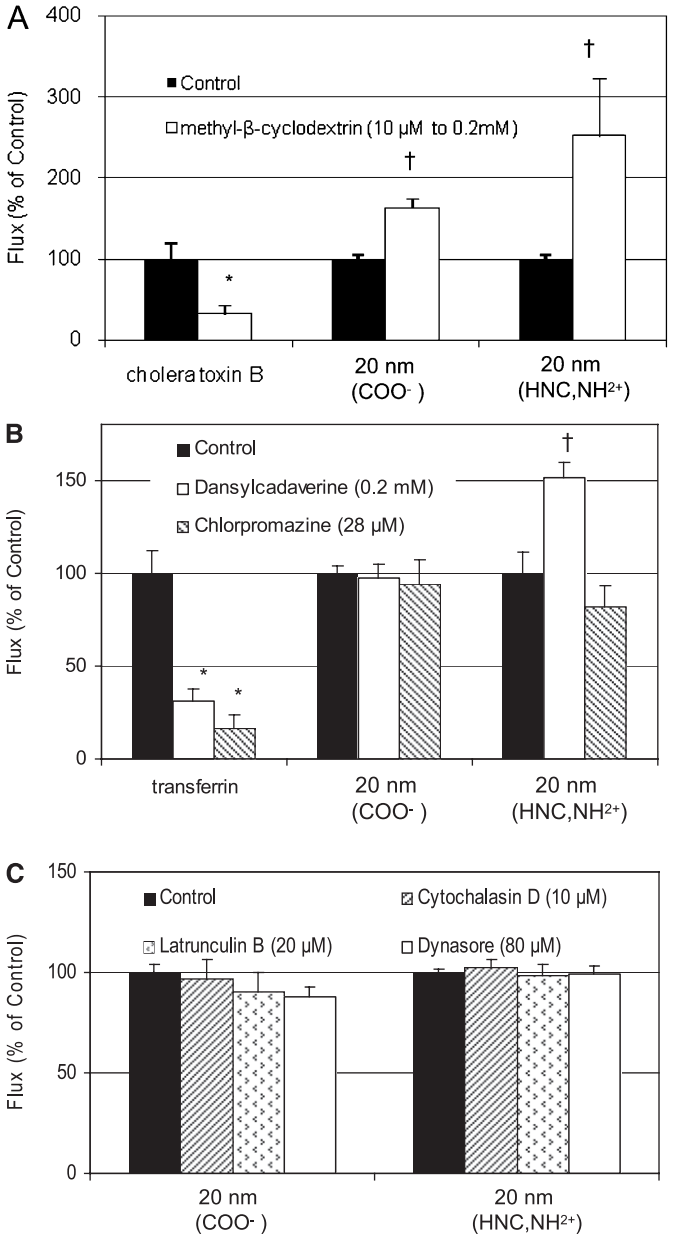

Figure 2. Effects of endocytosis inhibitors on PNP (amidine-modified and carboxylate-modified) flux across the RAECM. PNP flux was measured in the presence and absence of methyl-β-cyclodextrin (caveolin-mediated endocytosis inhibitor; *Panel A* (n = 11–13)), chlorpromazine or dansylcadaverine (clathrin-mediated endocytosis inhibitors; *Panel B* (n = 7–12)), latrunculin B or cyctochalasin D (phagocytosis and macropinocytosis inhibitors; *Panel C* (n = 8–9)), and dynasore (dynamin inhibitor; *Panel C* (n = 5)). FITC–cholera toxin B (CTB) (50 μg/ml apical concentration; *Panel A* (n = 5)) and Alexa 594–transferrin (500 μg/ml apical concentration; *Panel B* (n = 6)) flux across RAECMs was measured as positive control for caveolin- or clathrin-mediated endocytosis, respectively. *Significantly less than control; †significantly greater than control.

of nanoparticles yielded a linear relationship, the slope of which was used as a measure of relative PNP hydrophobicity.

Relative hydrophobicity of PNPs was also determined by the microbial adhesion to hydrocarbon (MATH) test with laboratory-grade decane (Sigma), using a protocol modified from Rosenberg (30). Samples were prepared by adding 4 ml of PNP solution in water at a concentration

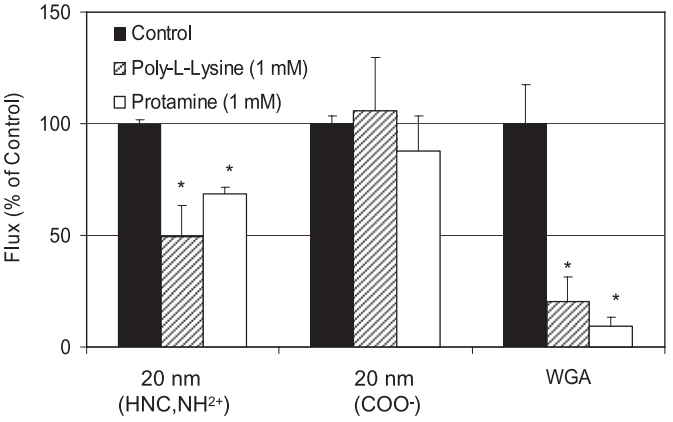

Figure 3. Effects of cationic polypeptides on 20 nm PNP (amidine-modified and carboxylate-modified) and wheat germ agglutinin (WGA) flux across RAECM. Flux was measured in the presence and absence of protamine (n = 5–8) or poly-l-lysine (n = 5–10). *Significantly less than control.

of 15 μg/ml to glass tubes containing 1 ml of decane. The tubes were vortexed (VWR, West Chester, PA) for 2 minutes, followed by 15 minutes of phase separation. Relative hydrophobicity (% MATH) was calculated as fraction of initial PNPs that partitioned into the decane phase from the aqueous phase.

PNP Zeta Potential

PNP zeta potential was determined using a Zetasizer (Malvern, Worcestershire, UK). The measurement cell (with built-in electrodes) was filled with 1 ml of various PNPs suspended in water at 176 μg/ml and loaded into the Zetasizer. Zeta potentials were estimated by applying an electric field across the two electrodes.

Data Analysis

Data are presented as means ±SEM. Comparisons of multiple group means, one-way or two-way analyses of variance, followed by *post hoc* procedures based on modified Newman-Keuls tests, were performed with GB-STAT v9.0 software (Dynamic Microsystems, Silver Spring, MD). Student's t tests were used for comparisons of two group means. $P < 0.05$ was considered statistically significant.

RESULTS

Exposure of RAECM to 2 mM EGTA decreased Rt by greater than 90% and greater than 95% at 2 and 24 hours, respectively. Flux of 20 nm carboxylate- or amidine-modified PNPs (at apical [PNPs] of 176 μg/ml) across RAECM was not significantly different in the presence or absence of EGTA (Figure 1A). Trafficking rates of positively charged PNPs were 20–40 times those of negatively charged PNPs across RAECMs in the presence or absence of EGTA. The fraction of initial apical PNPs (20 nm, amidine- and carboxylate-modified) translocated (apical-to-basolateral) after 24 hours was very low at less than 2 and 0.1% for positively and negatively charged PNPs, respectively. Flux of amidine- or carboxylate-modified PNPs (20 nm) was 2–3 times greater than flux of amidine- or carboxylate-modified PNPs (100–120 nm), respectively, in agreement with our recently published data (17). Flux of 100 or 120 nm PNPs was similarly not different in the presence or absence of EGTA (data not shown). Figure 1B shows confocal micrographs of intracellular PNPs in RAECMs with and without exposure to 2 mM EGTA. PNPs are observed intracellularly under both conditions, although some zonula occludens-1 rearrangement is noted in the presence of EGTA.

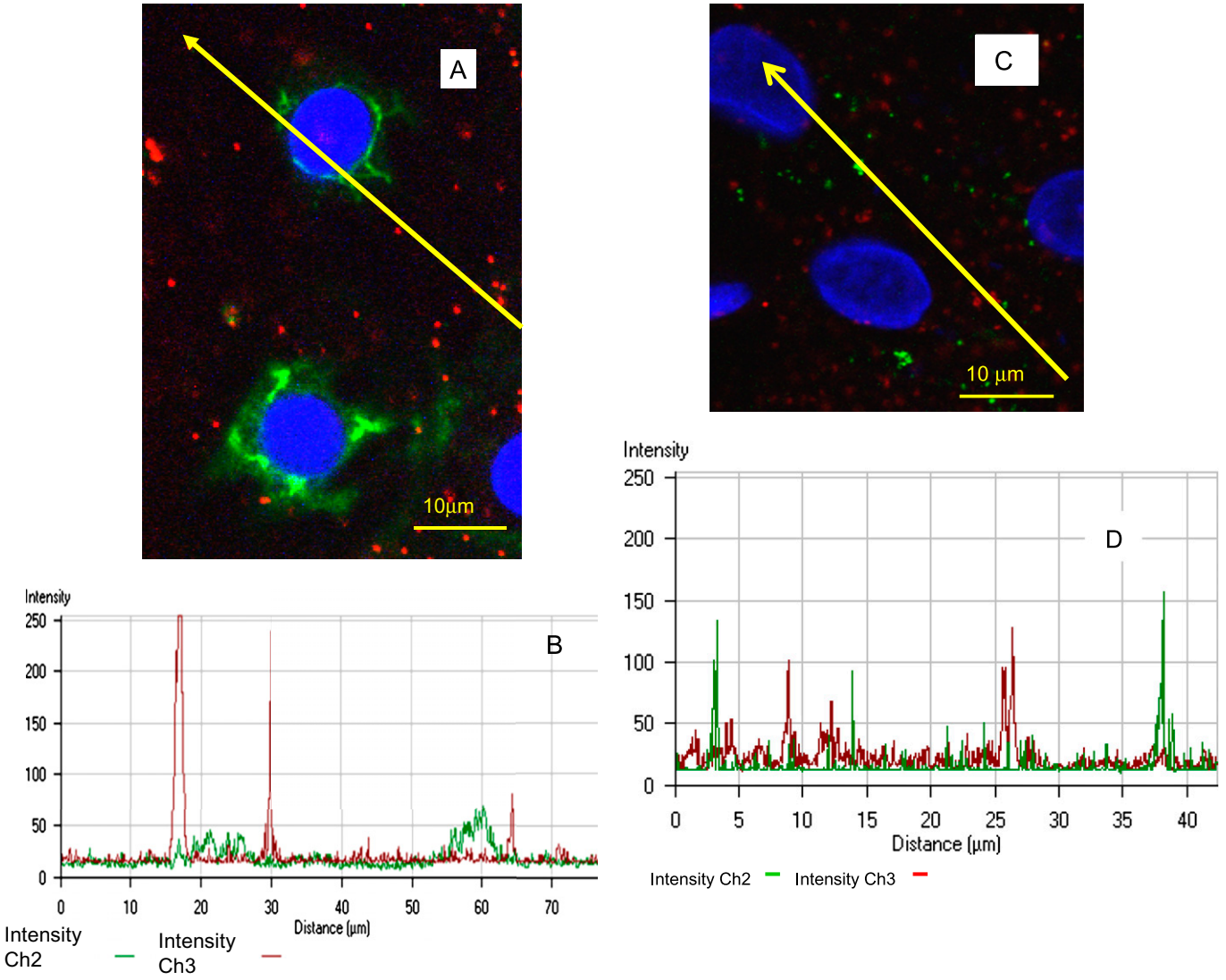

Figure 4. Absence of colocalization of PNPs with CTB (*Panels A* and *B*), caveolin-1 (*Panels C* and *D*) and clathrin heavy chain (*Panels E* and *F*). In *A* and *E*, midsection confocal photomicrographs show noncolocalization of internalized PNPs (100 nm, carboxylate-modified, *red*) with Alexa 488-CTB (*green*; *Panel A*) or clathrin heavy chain (*green*; *Panel E*) in RAECM after 1 hour of apical exposure. In *C*, the midsection confocal photomicrograph shows noncolocalization of internalized PNPs (120 nm, amidine-modified, *green*) with caveolin-1 (*red*) in RAECM after 1 hour of apical exposure. The profiling paths (*yellow arrows*) on the confocal images (*A, C,* and *E*) were translated into the corresponding intensity profile maps for PNPs (*red* in *Panels B* and *F*; *green* in *Panel D*), CTB (*green* in *Panel B*), caveolin-1 (*red* in *Panel D*), or clathrin heavy chain (*green* in *Panel F*). Each channel in *B*, *D*, and *F* shows peaks of fluorescence intensity, and corresponds to locations where PNPs, CTB, caveolin-1, or clathrin heavy chain were present.

Flux of carboxylate- or amidine-modified (20 nm) PNPs (at apical [PNPs] of 176 μg/ml) across RAECM did not decrease after monolayers were treated with methyl-β-cyclodextrin, dansylcadaverine, chlorpromazine, latrunculin B, cytochalasin D, or dynasore (Figure 2). Flux of amidine- or carboxylate-modified PNPs (20 nm) at baseline was 58.68 ±6.53 and 2.34 (±0.18) pg/cm^2/s, respectively. Flux of amidine-modified (120 nm) and carboxylate-modified (100 nm) PNPs similarly did not decrease in the presence of these inhibitors (data not shown). In contrast, flux of CTB decreased by 75% in the presence of methyl-β-cyclodextrin (positive control, Figure 2A). Flux of CTB across RAECMs at baseline was 2.15 ±1.08 pg/cm^2/s. Transferrin flux decreased in the presence of dansylcadaverine or chlorpromazine by approximately 75 and 85%, respectively (positive control, Figure 2B). Flux of transferrin across RAECMs at baseline was 35.93 ±9.53 pg/cm^2/s. Flux of either positively or negatively charged PNPs increased when monolayers were pretreated with methyl-β-cyclodextrin (10–200 μM). Additionally, flux of positively, but not negatively, charged PNPs increased in the presence of dansylcadaverine. Exposure to chlorpromazine (28 μM) and dansylcadaverine (200 μM) did not change Rt over 24 hours (data not shown). Methyl-β-cyclodextrin (10–200 μM), cyctochalasin D (10 μM), and latrunculin B (20 μM) exposure decreased Rt by approximately 40–65% over 24 hours (data not shown). Dynasore (80 μM) exposure increased Rt approximately 50% over 24 hours (data not shown).

RAECM treatment with protamine or poly-l-lysine decreased amidine-modified 20 nm PNPs and WGA flux and did not affect carboxylate-modified PNPs (20 nm) flux (Figure 3). Flux of amidine- and carboxylate-modified PNPs (20 nm) and WGA across RAECM at baseline was 38.78 ± 4.01, 1.29 ± 0.07 and 36.4 ± 6.39 pg/cm^2/s, respectively. Similarly, RAECM exposure to these polypeptides decreased amidine-modified 120 nm PNPs

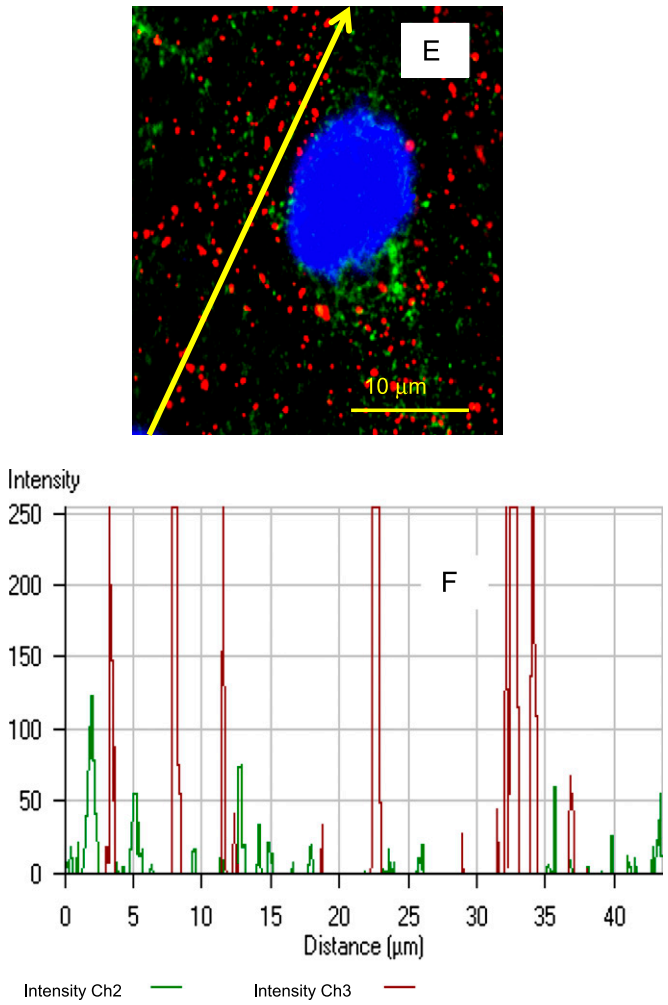

Figure 4. (*continued*)

flux and did not decrease carboxylate-modified 100 nm flux (data not shown). Although RAECM exposure to these polypeptides decreased amidine-modified PNP flux, trafficking rates of amidine-modified PNPs remained 10–15 times those of similarly sized carboxylate-modified PNPs. RAECM treatment with poly-l-lysine (1 mM) or protamine (1 mM) decreased Rt up to 80% over 24 hours of exposure (data not shown).

We investigated colocalization of PNPs with CTB, caveolin-1 or clathrin heavy chain by CLSM (Figure 4). Carboxylate-modified PNPs (100 nm) did not colocalize with Alexa 488-CTB (Figures 4A and 4B), caveolin-1 (data not shown) or clathrin heavy chain (Figures 4E and 4F) in RAECM after 1 hour of apical exposure. Amidine-modified PNPs (120 nm) did not colocalize with Alexa 594-CTB (data not shown), caveolin-1 (Figures 4C and 4D) or clathrin heavy chain (data not shown) after 1 hour of apical exposure.

Figure 5 shows lack of colocalization of amidine-modified PNPs (120 nm) and EEA1 (Figures 5A and 5B) or WGA (Figures 5C and 5D). Similar lack of colocalization of EEA1 or WGA with carboxylate-modified PNPs (100 nm) was observed (data not shown). WGA highly colocalized with EEA1 after 1 hour of exposure (positive control, Figures 5E and 5F). Similarly, CTB showed strong colocalization with EEA1 after 1 hour of exposure (data not shown). These data in aggregate, revealing no effect of endocytosis inhibitors on PNP flux and absence of colocalization of PNPs with EEA1, caveolin-1, clathrin heavy chain, CTB and WGA, are all consistent with the conclusion that PNP transport is not mediated by the major known endocytosis pathways.

Table 1 summarizes relative hydrophobicity of amidine-modified (20 and 120 nm) and carboxylate-modified (20 and 100 nm) PNPs, as estimated by Rose Bengal distribution and MATH test, and PNP zeta potentials in water. Amidine-modified PNPs (20 or 120 nm) were relatively much more hydrophobic than carboxylate-modified PNPs (20 or 100 nm).

Figure 6 shows PNP (carboxylate-modified (20 and 100 nm) and amidine-modified (20 and 120 nm)) trafficking rates across RAECMs and ALBFs over 24 hours at [PNPs] of 176 μg/ml in the apical (upper) fluid. Trafficking rates for positively charged (amidine-modified) PNPs are 20–40 times greater than those for comparably-sized negatively charged (carboxylate-modified) PNPs across both RAECMs and ALBFs. Smaller (20 nm) PNPs were transported approximately two- to three-times faster than larger (100 or 120 nm) PNPs with similar net surface charge density across both RAECMs and ALBFs. Translocation of PNPs across RAECMs was two- to three-times faster than that across ALBFs.

Efflux of 5-CFDA from AECs into apical fluid in the presence or absence of RAECM exposure to amidine- or carboxylate-modified PNPs (176 μg/ml; 20, 100, or 120 nm) or 0.1% TX-100 (positive control) is summarized in Table 2. At 30 minutes or 2 hours (data not shown) after RAECM exposure, ΔF in the presence of TX-100 was significantly higher than that in the presence or absence of PNPs. No significant differences in ΔF were seen in the presence and absence of PNPs. P_{app} of ^{22}Na or ^{14}C-mannitol measured in the presence and absence of exposure of ALBFs to amidine- or carboxylate-modified PNPs (176 μg/ml; 20 nm) are summarized in Table 3. P_{app} of neither ^{22}Na nor ^{14}C-mannitol was altered by PNP (20 nm) exposure. Similarly, P_{app} of ^{14}C-mannitol in the presence and absence of amidine- or carboxylate-modified PNPs (176 μg/ml; 120 or 100 nm) did not change significantly (data not shown). These data suggest that PNP translocation across RAECMs or ALBFs does not create pathways in the lipid bilayer of cell plasma membranes that allow enhanced transport of small ions/molecules.

DISCUSSION

In this study, we demonstrate that PNPs are translocated across RAECMs in the apical-to-basolateral direction transcellularly, primarily via nonendocytic pathways. Our data indicate no change in PNP trafficking rates or pathways after RAECM exposure to EGTA. We did not observe decreased PNP trafficking rates after exposure to inhibitors of the major known endocytosis pathways, consistent with the lack of colocalization between PNPs and early endosome marker (EEA1), caveolin-1, clathrin heavy chain, CTB, or WGA. PNP trafficking of positively charged PNPs was 20–40 times that of negatively charged PNPs across both RAECMs and ALBFs, whereas trafficking rates across RAECMs were 2–3 times faster than those across ALBFs. These data suggest that PNPs translocate primarily transcellularly across RAECMs, but not via known major endocytic pathways, possibly by direct interaction with the lipid bilayer of cell plasma membranes.

In general, nanoparticles may be taken up into cells (and perhaps eventually transcytosed) via endocytosis (31). There are also nonendocytic mechanisms by which nanoparticles may enter and traffic across cell monolayers: across paracellular pathways (tight junctions), through "holes" (or defects) in the plasma membrane, or by passive or facilitated diffusion across the plasma membrane. It has been shown that hydrophilic solutes (Stokes-Einstein radii, <6 nm) may passively translocate by restricted diffusion via paracellular pathways (32, 33).

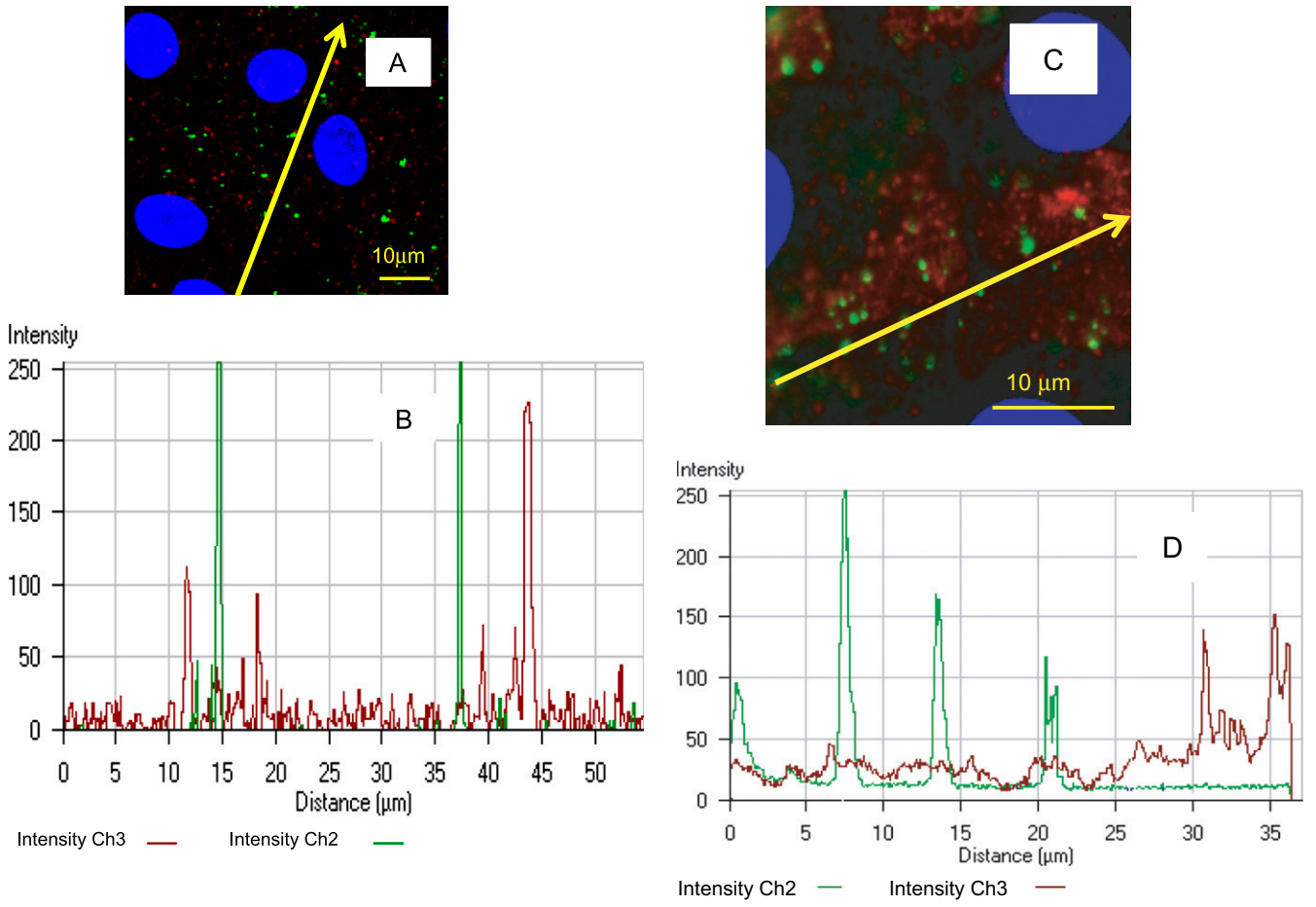

Figure 5. Absence of colocalization of PNPs with early endosome antigen–1 (EEA1) (*Panels A* and *B*) or WGA (*Panels C* and *D*). Midsection confocal photomicrographs show noncolocalization of internalized PNPs (120 nm, amidine-modified, *green*) with EEA1 (*red* in *Panel A*) or WGA (*red* in *Panel C*) in RAECM after 1 hour of apical PNP exposure. In *E*, the midsection confocal micrograph shows colocalization of WGA (*red*) with EEA1 (*green*) in RAECM after 1 hour of apical WGA exposure. The profiling paths (*yellow arrows*) on the confocal images (*A, C,* or *E*) were translated into the corresponding intensity profile maps for PNPs (*green* in *Panels B* and *D*), EEA1 (*red* in *Panel B* and *green* in *Panel F*), or WGA (*red* in *Panels D* and *F*). *Green* and *red* channels show peaks of fluorescence intensity, and correspond to locations where PNPs, EEA1, or WGA were present. Each channel in *B, D,* and *F* show peaks of fluorescence intensity, and corresponds to locations where PNPs, EEA1, or WGA were present.

Several reports on passive diffusion of hydrophilic solutes in many epithelial barriers indicate that paracellular pathways can be modeled to have equivalent water-filled pores, the radii of which range from 5 to 6 nm (33). It is reasonable to predict that nanoparticles of less than 10 nm may diffuse from airspaces between epithelial cells into interstitium (and eventually reaching the systemic circulation), while particles of greater than 10 nm are expected to be excluded from tight junctions under normal conditions. However, if specific nanoparticles affect the epithelial barrier so as to open junctions between epithelial cells, nanoparticle diffusion via such altered tight junctions could be increased. Treatment with EGTA increases the equivalent pore size of tight junctions in epithelia and increases permeability of mannitol (180 Da (~0.82 nm)) and dextran (2 KDa (~2.22 nm), 4 KDa (~2.8 nm), or 12 KDa (4.03 nm)) (34, 35). Trafficking rates of PNPs used in this study (20 and 100 nm) did not increase in the presence of EGTA. Confocal micrographs of RAECMs exposed to EGTA confirm the presence of PNPs inside cells and not in cell–cell junctions. Because relatively high PNP concentrations were used, presumably some agglomeration occurred in culture media and/or within cells. However, the fact that 20 nm PNPs traffic 2–3 times faster than 100 to 120 nm PNPs with similar surface charge across RAECMs, as well as across ALBFs, suggests that individual PNPs were likely the predominant form by which uptake/trafficking takes place. These results indicate that PNPs cross RAECMs transcellularly, both in the presence and absence of EGTA.

The lung is richly endowed with caveolae, especially in ATI cells (23). The most effective way to disrupt caveolar function is with sterol-binding drugs that sequester cholesterol (a prominent component of lipid rafts involved in caveolae formation), including methyl-β-cyclodextrin (23). Methyl-β-cyclodextrin markedly decreases CTB flux, while increasing PNP (20, 100, or 120 nm, carboxylate- or amidine-modified) flux across RAECMs. Cholesterol depletion due to pretreatment of monolayers with methyl-β-cyclodextrin may have led to increased membrane fluidity and resultant increases in PNP flux (36). Carboxylate-modified PNPs (24 nm) are taken up at a higher rate into HeLa cells in the presence of methyl-β-cyclodextrin (37), suggesting that cholesterol depletion may increase cellular entry via pathways that are less readily available under normal conditions. Dausend and colleagues (38) recently demonstrated that cholesterol depletion does not decrease positively or negatively charged PNP (120 nm) uptake into Hela cells. We did not observe colocalization between PNPs and CTB or

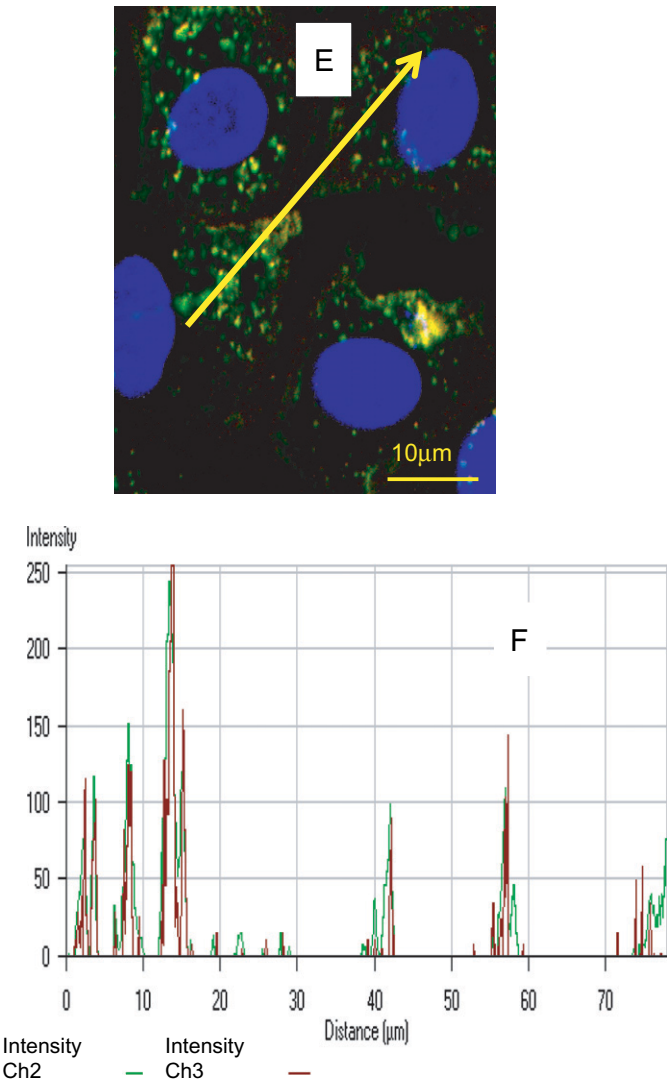

Figure 5. (*continued*)

caveolin-1, confirming our flux measurements and indicating that PNPs do not use the caveolin-mediated endocytosis pathway in RAECMs. Since caveolin-1 expression and caveolar biogenesis are prominent in ATI but not in ATII cells (39), similar transport rates of PNPs across ATII and ATI cell-like RAECMs (17) is consistent with the conclusion that PNPs do not use caveolin-mediated endocytosis. Kemp and colleagues (40) recently showed that human ATI and ATII-like cells both take up positively and negatively charged PNPs (50 nm) without utilizing the caveolin-mediated pathway although, in their studies, a significant difference in rate of PNP uptake in type I and II cells was noted.

In clathrin-mediated endocytosis, cargo is recognized by adapter protein complexes that in turn recruit a clathrin coat with the help of other effector proteins. Internalization is followed by uncoating of clathrin and fusion of vesicles with other endosomal membranes. Dansylcadaverine or chlorpromazine are two inhibitors of clathrin-dependent endocytosis (20–22). Chlorpromazine causes clathrin and AP-2 to relocate to multivesicular bodies and, by relocating clathrin-coated pits, inhibits clathrin-mediated endocytosis (22). The mechanism of action of dansylcadaverine is not fully understood. Some evidence indicates that dansylcadaverine inhibits receptor trafficking at a step proximal to the formation of endocytic vesicles (20) and inhibits formation of clathrin-coated pits. Since RAECM exposure to chlorpromazine or dansylcadaverine leads to a decrease in transferrin flux but no decrease in amidine- or carboxylate-modified PNP (20, 100 or 120 nm) flux and absence of PNP colocalization with clathrin heavy chain by CLSM, we conclude that PNPs do not use the clathrin-mediated endocytosis pathway.

Dynamin is a GTP-dependent enzyme that wraps around invaginations of the cell membrane as a coil-like structure during the budding process in endocytosis, constricting the neck by GTP hydrolysis and thereby pinching off the vesicle. Dynamin is known to be involved in different endocytic processes, including clathrin- and caveolin-mediated endocytosis. Our results utilizing dynasore revealed no change in PNP flux, suggesting PNP transport across RAECMs is a dynamin-independent process. Dausend and colleagues (38) showed that positively and negatively charged PNP (120 nm) transport across HeLa cells is dynamin dependent. These data and other reports on PNP trafficking across epithelial barriers (40, 41) indicate that mechanisms of PNP transport are both cell type–specific and dependent on the physicochemical properties of PNPs.

Macropinocytosis is a nonspecific internalization mechanism that is inhibited by F-actin disruption by targeting agents such as cyctochalasin D and latrunculin B (21). Phagocytosis is associated with uptake in macrophages and dendritic cells, but can be induced in most cells by expression of the requisite receptors (42). There have been a few reports of ATI and ATII cell phagocytosis (43). Phagocytosis also relies on the actin cytoskeleton (21). Our results show that RAECM exposure to cyctochalasin D or latrunculin B did not decrease PNP (amidine- or carboxylate-modified, 20, 100, or 120 nm) flux, suggesting that PNP transport across RAECMs does not use the macropinocytosis or phagocytosis pathways. The absence of PNP colocalization with early endosome marker, EEA1, confirms that PNP trafficking does not use known endocytosis pathways. Geiser and colleagues (44) also demonstrated that F-actin disruption does not decrease PNP uptake into porcine lung macrophages, consistent with a nonendocytic uptake mechanism.

TABLE 1. RELATIVE HYDROPHOBICITY AND ZETA POTENTIAL OF CARBOXYLATE- AND AMIDINE-MODIFIED POLYSTYRENE NANOPARTICLES

PNPs	Relative Hydrophobicity ($\mu m^{-2} \times 10^{-14}$)	Hydrophobicity (*% MATH*)	Zeta Potential in Water (*mV*)
20 nm (amidine-modified)	37,700 ± 2,152	44 ± 10	71 ± 7
120 nm (amidine-modified)	2,000 ± 707	51 ± 2	67 ± 12
20 nm (carboxylate-modified)	73 ± 11	3 ± 1	45 ± 19
100 nm (carboxylate-modified)	33 ± 41	0	53 ± 11

Definition of abbreviations: MATH, microbial adhesion to hydrocarbon; PNPs, polystyrene nanoparticles.

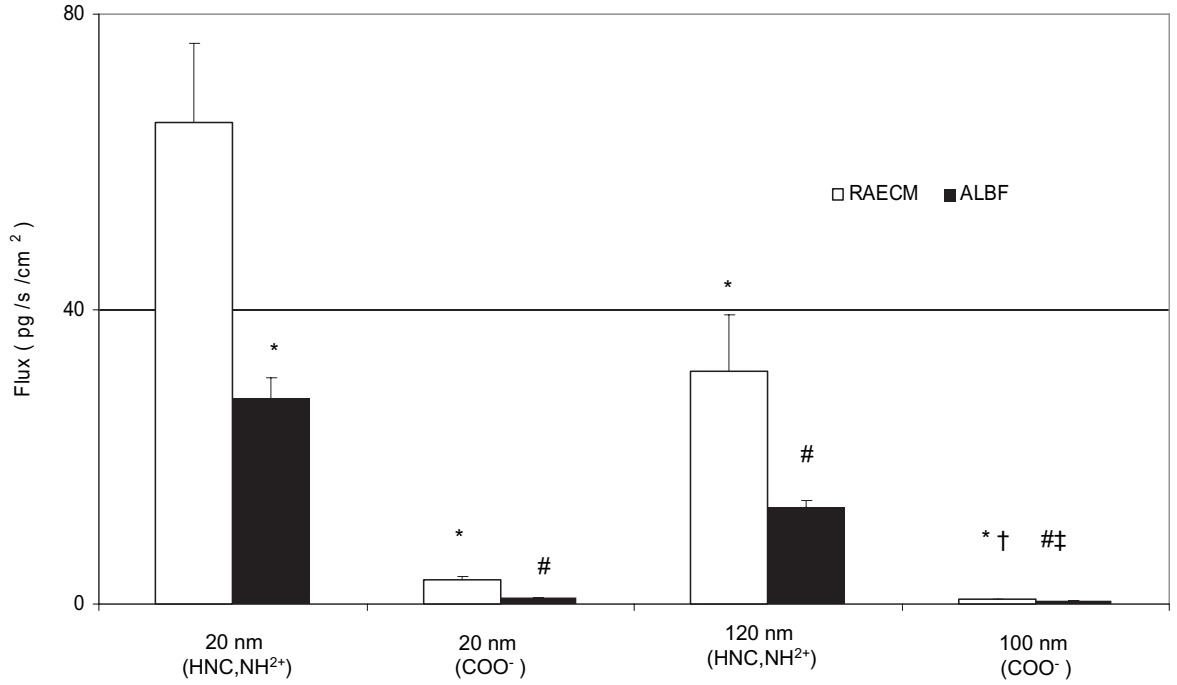

Figure 6. Positively (amidine-modified, 20 and 120 nm) and negatively (carboxylate-modified, 20 and 100 nm) charged PNP flux across RAECM and artificial lipid bilayers on filters (ALBFs). Monolayers were exposed to 176 μg/ml apical PNPs at time 0 (n = 6–13). *Significantly less than positively charged 20 nm PNP flux across RAECM; #significantly less than positively charged 20 nm PNP flux across ALBFs; †significantly less than positively charged 120 nm PNP flux across RAECM; ‡significantly less than positively charged 120 nm PNP flux across ALBFs.

Because of the net negative charge of cell plasma membranes (e.g., due to glycoproteins/glycosphingolipids), nonspecific interaction of some cationic peptides/ligands with cell membranes could lead to nonspecific adsorptive endocytosis (27). Adsorptive endocytosis is initiated by nonspecific physical adsorption to the cell surface by electrostatic forces, followed by invagination of the local plasma membrane, to form intracellular vesicles. Because specific receptors are not required, adsorptive endocytosis mainly relies on size and surface properties of the adsorbed material and the cell surface areas available (45). Polycationic substances, such as protamine or poly-l-lysine, have been shown to compete with cationic peptides/particles for cell membrane binding, and inhibit their uptake in different cell types (26, 27). Our data show that exposure to poly-l-lysine or protamine causes significant decreases (30–50%) in amidine-modified PNP (20 or 120 nm) flux, although the flux ratio of positively charged to negatively charged PNPs remains high (~10–15 times). These data, together with those showing absence of intracellular colocalization of PNPs and EEA1 or WGA, suggest that neither amidine-modified nor carboxylate-modified PNP transcytosis occurs via adsorptive endocytosis.

Computer simulation modeling and experimental evidence have indicated that increased (nano)particle surface hydrophobicity increases uptake rates into cells (29, 46–48). Amidine-modified PNPs are relatively much more hydrophobic than carboxylate-modified PNPs, suggesting that the higher rate of trafficking of amidine-modified PNPs compared with carboxylate-modified PNPs across RAECMs and ALBFs may be related to their relative hydrophobicities.

"Holes" (or defects) in lipid bilayers have been reported to be created by interactions of certain classes of nanoparticles with lipid components of cell membranes (49, 50). The term "hole" can refer to a wide range of structural changes in the plasma membrane, including formation of a transient opening, or slight changes in content of the membrane, leading to enhanced diffusion (51). Cationic polymeric nanoparticles (e.g., poly(amidoamine) dendrimers), in particular, were reported to create relatively large holes (~10–40 nm) in lipid bilayers, allowing enhanced uptake of nanoparticles and leakage of cellular enzymes (e.g., lactate dehydrogenase) (49, 50). In contrast, it has been shown previously that some macromolecules/nanoparticles can penetrate the plasma membrane with-

TABLE 2. EFFLUX OF 5-CARBOXYFLUORESCEIN DIACETATE FROM RAT ALVEOLAR EPITHELIAL CELL MONOLAYERS

	PNP					
	20 nm		100 nm			
ΔF	(Amidine-modified)	(Carboxylate-modified)	(Amidine-modified)	(Carboxylate-modified)	Negative Control (No PNP)	Positive Control (0.1% TX-100)
30 min	3.1 ± 0.8	2.1 ± 1.0	1.5 ± 0.7	2.7 ± 1.2	3.8 ± 0.9	23.9 ± 7.3*

Definition of abbreviations: ΔF, efflux of 5-carboxyfluorescein diacetate; PNP, polystyrene nanoparticles; TX-100, Triton X-100.

Effects of rat alveolar epithelial cell monolayer exposure to apical PNP (176 μg/ml) on 5-carboxyfluorescein diacetate leakage into apical fluid after 30 minutes (ΔF). ΔF values are shown as means ±SEM (n = 6). No significant differences in ΔF in the presence or absence of PNPs were seen.

* Significantly greater than ΔF in the presence or absence of PNP.

TABLE 3. APPARENT PERMEABILITY OF MANNITOL AND SODIUM ACROSS ARTIFICIAL LIPID BILAYER ON FILTER

P_{app} ($\times 10^{-9}$ cm/s)	Control (No PNP)	20 nm PNPs (Amidine-modified)	20 nm PNPs (Carboxylate-modified)
^{22}Na	6.30 ± 3.32	5.54 ± 1.66	5.05 ± 2.38
^{14}C-mannitol	8.32 ± 1.32	8.23 ± 1.40	8.54 ± 1.18

Definition of abbreviations: P_{app}, apparent permeability; PNPs, polystyrene nanoparticles.

Effects of exposure to apical PNP (176 μg/ml) on P_{app} ($\times 10^{-9}$ cm/s) of ^{22}Na and ^{14}C-mannitol across artificial lipid bilayers. P_{app} are shown as means (±SEM) ($n = 7$). No significant differences due to PNP exposure were seen.

out membrane poration (52, 53). PNPs did not promote leakage of 5-CFDA from RAECMs, whereas mannitol and sodium permeability across ALBFs did not change in the presence or absence of PNPs, indicating that PNP transport does not create transient "holes" (or defects) in plasma membranes, and suggesting that PNPs directly interact with the lipid bilayer of plasma membranes.

In conclusion, we have shown that PNP translocation across RAECMs takes place primarily through transcellular pathways that do not appear to involve endocytosis. Higher trafficking rates of amidine-modified PNPs compared with carboxylate-modified PNPs are dependent on their surface charge and/or relative hydrophobicity, suggesting that direct interactions between PNPs and cell membranes may be the predominant mechanism for PNP internalization from apical fluid into pneumocytes, and eventual transfer to basolateral fluid. Our data are most consistent with translocation of PNPs by direct penetration through the lipid bilayer of cell plasma membranes without membrane poration. Findings from these studies provide further insight into nanomaterial uptake into cells, and may help lead to new approaches to drug/gene delivery to lung epithelial cells after nanoparticle inhalation.

Conflict of Interest Statement: N.M. has sponsored grants from the National Institutes of Health (NIH) ($100,000 or more), the National Science Foundation ($100,000 or more), and the American Cancer Society ($10,001–$50,000). L.D. has received a junior scientist development grant from the American Heart Association ($75,000 per annum over the last 4 years). S.F.H.-A. has received a research grant to investigate mechanisms of drug action on exocytosis in lacrimal gland from Alcon ($100,000 or more) and a grant from NIH ($100,000 or more). Z.B. has received sponsored grants from NIH ($100,000 or more). K.-J.K. has received royalties from Springer for book editing (more than $1,000). E.C. has received sponsored grants from NIH (more than $100,000). None of the other authors has a financial relationship with a commercial entity that has an interest in the subject of this manuscript.

Acknowledgments: The authors appreciate helpful discussions with Herbert J. Meiselman, Ph.D., Tamas Alexy, M.D., and Leena Petal, Ph.D., and the expert technical assistance of Juan Raymond Alvarez and David Winter. E.D.C. is Hastings Professor and Kenneth T. Norris, Jr. Chair of Medicine. Z.B. is Ralph Edgington Chair in Medicine.

References

1. Oberdorster G, Maynard A, Donaldson K, Castranova V, Fitzpatrick J, Ausman K, Carter J, Karn B, Kreyling W, Lai D, *et al.* Principles for characterizing the potential human health effects from exposure to nanomaterials: elements of a screening strategy. *Part Fibre Toxicol* 2005;2:8.
2. Sun Q, Wang A, Jin X, Natanzon A, Duquaine D, Brook RD, Aguinaldo JG, Fayad ZA, Fuster V, Lippmann M, *et al.* Long-term air pollution exposure and acceleration of atherosclerosis and vascular inflammation in an animal model. *JAMA* 2005;294:3003–3010.
3. Yacobi NR, Phuleria HC, Demaio L, Liang CH, Peng CA, Sioutas C, Borok Z, Kim KJ, Crandall ED. Nanoparticle effects on rat alveolar epithelial cell monolayer barrier properties. *Toxicol In Vitro* 2007;21:1373–1381.
4. Furuyama A, Kanno S, Kobayashi T, Hirano S. Extrapulmonary translocation of intratracheally instilled fine and ultrafine particles via direct and alveolar macrophage-associated routes. *Arch Toxicol* 2009;83:429–437.
5. Cheek JM, Evans MJ, Crandall ED. Type I cell–like morphology in tight alveolar epithelial monolayers. *Exp Cell Res* 1989;184:375–387.
6. Evans MJ, Cabral LJ, Stephens RJ, Freeman G. Transformation of alveolar type 2 cells to type 1 cells following exposure to NO_2. *Exp Mol Pathol* 1975;22:142–150.
7. Yang W, Peters JI, Williams RO III. Inhaled nanoparticles—a current review. *Int J Pharm* 2008;356:239–247.
8. Crandall ED, Matthay MA. Alveolar epithelial transport: basic science to clinical medicine. *Am J Respir Crit Care Med* 2001;163:1021–1029.
9. Kim KJ, Malik AB. Protein transport across the lung epithelial barrier. *Am J Physiol* 2003;284:L247–L259.
10. Widera A, Kim KJ, Crandall ED, Shen WC. Transcytosis of GCSF-transferrin across rat alveolar epithelial cell monolayers. *Pharm Res* 2003;20:1231–1238.
11. Danto SI, Zabski SM, Crandall ED. Reactivity of alveolar epithelial cells in primary culture with type I cell monoclonal antibodies. *Am J Respir Cell Mol Biol* 1992;6:296–306.
12. Kansy M, Senner F, Gubernator K. Physicochemical high throughput screening: parallel artificial membrane permeation assay in the description of passive absorption processes. *J Med Chem* 1998;41:1007–1010.
13. Kwon JH, Katz LE, Liljestrand HM. Use of a parallel artificial membrane system to evaluate passive absorption and elimination in small fish. *Environ Toxicol Chem* 2006;25:3083–3092.
14. Ottaviani G, Martel S, Carrupt PA. Parallel artificial membrane permeability assay: a new membrane for the fast prediction of passive human skin permeability. *J Med Chem* 2006;49:3948–3954.
15. Kikkawa Y, Yoneda K, Smith F, Packard B, Suzuki K. The type II epithelial cells of the lung. II. Chemical composition and phospholipid synthesis. *Lab Invest* 1975;32:295–302.
16. Schmidt-Sommerfeld E, Borer RC. Biochemical characterization of clonally isolated and continuously cultured type II cells from adult rat lung. *Am Rev Respir Dis* 1979;120:1145–1148.
17. Yacobi NR, Demaio L, Xie J, Hamm-Alvarez SF, Borok Z, Kim KJ, Crandall ED. Polystyrene nanoparticle trafficking across alveolar epithelium. *Nanomedicine* 2008;4:139–145.
18. Borok Z, Danto SI, Zabski SM, Crandall ED. Defined medium for primary culture de novo of adult rat alveolar epithelial cells. *In Vitro Cell Dev Biol Anim* 1994;30A:99–104.
19. Kim KJ, Crandall ED. Models for investigation of peptide and protein transport across cultured mammalian respiratory epithelial barriers. *Pharm Biotechnol* 1996;8:325–346.
20. Davies PJ, Cornwell MM, Johnson JD, Reggianni A, Myers M, Murtaugh MP. Studies on the effects of dansylcadaverine and related compounds on receptor-mediated endocytosis in cultured cells. *Diabetes Care* 1984;7:35–41.
21. Ivanov AI. Pharmacological inhibition of endocytic pathways: is it specific enough to be useful? *Methods Mol Biol* 2008;440:15–33.
22. Wang LH, Rothberg KG, Anderson RG. Mis-assembly of clathrin lattices on endosomes reveals a regulatory switch for coated pit formation. *J Cell Biol* 1993;123:1107–1117.
23. Parton RG, Richards AA. Lipid rafts and caveolae as portals for endocytosis: new insights and common mechanisms. *Traffic* 2003;4:724–738.
24. Kirchhausen T, Macia E, Pelish HE. Use of dynasore, the small molecule inhibitor of dynamin, in the regulation of endocytosis. *Methods Enzymol* 2008;438:77–93.
25. Chen B, Liu Q, Zhang Y, Xu L, Fang X. Transmembrane delivery of the cell-penetrating peptide conjugated semiconductor quantum dots. *Langmuir* 2008;24:11866–11871.
26. Behrens I, Pena AI, Alonso MJ, Kissel T. Comparative uptake studies of bioadhesive and non-bioadhesive nanoparticles in human intestinal cell lines and rats: the effect of mucus on particle adsorption and transport. *Pharm Res* 2002;19:1185–1193.
27. Sai Y, Kajita M, Tamai I, Wakama J, Wakamiya T, Tsuji A. Adsorptive-mediated endocytosis of a basic peptide in enterocyte-like Caco-2 cells. *Am J Physiol* 1998;275:G514–G520.
28. Broadwell RD, Balin BJ, Salcman M. Transcytotic pathway for blood-borne protein through the blood-brain barrier. *Proc Natl Acad Sci USA* 1988;85:632–636.
29. Muller RH, Mehnert W, Hildebrand GE. Particle and surface characterisation methods, 1st ed. Guilford, UK: Medpharm Scientific Publishers; 1997.
30. Rosenberg M. Microbial adhesion to hydrocarbons: twenty-five years of doing MATH. *FEMS Microbiol Lett* 2006;262:129–134.

31. Conner SD, Schmid SL. Regulated portals of entry into the cell. *Nature* 2003;422:37–44.
32. Kim KJ, Crandall ED. Heteropore populations of bullfrog alveolar epithelium. *J Appl Physiol* 1983;54:140–146.
33. Matsukawa Y, Lee VH, Crandall ED, Kim KJ. Size-dependent dextran transport across rat alveolar epithelial cell monolayers. *J Pharm Sci* 1997;86:305–309.
34. des Rieux A, Fievez V, Momtaz M, Detrembleur C, Alonso-Sande M, Van Gelder J, Cauvin A, Schneider YJ, Preat V. Helodermin-loaded nanoparticles: characterization and transport across an *in vitro* model of the follicle-associated epithelium. *J Control Release* 2007;118: 294–302.
35. Gonzalez-Mariscal L, Contreras RG, Bolivar JJ, Ponce A, Chavez De Ramirez B, Cereijido M. Role of calcium in tight junction formation between epithelial cells. *Am J Physiol* 1990;259:C978–C986.
36. Yeagle PL. Cholesterol and the cell membrane. Boca Raton: CRC press; 1988.
37. Lai SK, Hida K, Man ST, Chen C, Machamer C, Schroer TA, Hanes J. Privileged delivery of polymer nanoparticles to the perinuclear region of live cells via a non-clathrin, non-degradative pathway. *Biomaterials* 2007;28:2876–2884.
38. Dausend J, Musyanovych A, Dass M, Walther P, Schrezenmeier H, Landfester K, Mailander V. Uptake mechanism of oppositely charged fluorescent nanoparticles in HeLa cells. *Macromol Biosci* 2008;8: 1135–1143.
39. Newman GR, Campbell L, von Ruhland C, Jasani B, Gumbleton M. Caveolin and its cellular and subcellular immunolocalisation in lung alveolar epithelium: implications for alveolar epithelial type I cell function. *Cell Tissue Res* 1999;295:111–120.
40. Kemp SJ, Thorley AJ, Gorelik J, Seckl MJ, O'Hare MJ, Arcaro A, Korchev Y, Goldstraw P, Tetley TD. Immortalization of human alveolar epithelial cells to investigate nanoparticle uptake. *Am J Respir Cell Mol Biol* 2008;39:591–597.
41. Xia T, Kovochich M, Liong M, Zink JI, Nel AE. Cationic polystyrene nanosphere toxicity depends on cell-specific endocytic and mitochondrial injury pathways. *ACS Nano* 2008;2:85–96.
42. Qualmann B, Mellor H. Regulation of endocytic traffic by Rho GTPases. *Biochem J* 2003;371:233–241.
43. Corrin B. Phagocytic potential of pulmonary alveolar epithelium with particular reference to surfactant metabolism. *Thorax* 1970;25:110–115.
44. Geiser M, Rothen-Rutishauser B, Kapp N, Schürch S, Kreyling W, Schulz H, Semmler M, Im Hof W, Heyder J, Gehr P. Ultrafine particles cross cellular membranes by nonphagocytic mechanisms in lungs and in cultured cells. *Environ Health Perspect* 2005;113:1555–1560.
45. Jung T, Kamm W, Breitenbach A, Kaiserling E, Xiao JX, Kissel T. Biodegradable nanoparticles for oral delivery of peptides: is there a role for polymers to affect mucosal uptake? *Eur J Pharm Biopharm* 2000;50:147–160.
46. des Rieux A, Ragnarsson EG, Gullberg E, Preat V, Schneider YJ, Artursson P. Transport of nanoparticles across an *in vitro* model of the human intestinal follicle associated epithelium. *Eur J Pharm Sci* 2005;25:455–465.
47. Li Y, Chen X, Gu N. Computational investigation of interaction between nanoparticles and membranes: hydrophobic/hydrophilic effect. *J Phys Chem B* 2008;112:16647–16653.
48. Wong-Ekkabut J, Baoukina S, Triampo W, Tang IM, Tieleman DP, Monticelli L. Computer simulation study of fullerene translocation through lipid membranes. *Nat Nanotechnol* 2008;3:363–368.
49. Hong S, Leroueil PR, Janus EK, Peters JL, Kober MM, Islam MT, Orr BG, Baker JR Jr, Banaszak Holl MM. Interaction of polycationic polymers with supported lipid bilayers and cells: nanoscale hole formation and enhanced membrane permeability. *Bioconjug Chem* 2006;17:728–734.
50. Mecke A, Majoros IJ, Patri AK, Baker JR Jr, Holl MM, Orr BG. Lipid bilayer disruption by polycationic polymers: the roles of size and chemical functional group. *Langmuir* 2005;21:10348–10354.
51. Leroueil PR, Hong S, Mecke A, Baker JR Jr, Orr BG, Banaszak Holl MM. Nanoparticle interaction with biological membranes: does nanotechnology present a Janus face? *Acc Chem Res* 2007;40: 335–342.
52. Patel LN, Zaro JL, Shen WC. Cell penetrating peptides: intracellular pathways and pharmaceutical perspectives. *Pharm Res* 2007;24: 1977–1992.
53. Verma A, Uzun O, Hu Y, Hu Y, Han HS, Watson N, Chen S, Irvine DJ, Stellacci F. Surface-structure–regulated cell-membrane penetration by monolayer-protected nanoparticles. *Nat Mater* 2008;7:588–595.